This is a preprint, the final version is subject to change, of the American Mineralogist (MSA)
Cite as Authors (Year) Title. American Mineralogist, in press.
(DOI will not work until issue is live.) DOI: http://dx.doi.org/10.2138/am-2017-5935

Revision 1:

Transformation of halloysite and kaolinite into beidellite under hydrothermal condition

Hongping He[1]*, Shichao Ji[1], Qi Tao[1], Jianxi Zhu[1], Tianhu Chen[2], Xiaoliang Liang[1], Zhaohui Li[3] and Hailiang Dong[4]

[1] Key Laboratory of Mineralogy and Metallogeny, Chinese Academy of Sciences & Guangdong Provincial Key Laboratory of Mineral Physics and Materials, Guangzhou Institute of Geochemistry, Guangzhou 510640, China

[2] School of Resources and Environmental Engineering, Hefei University of Technology, Hefei 230009, China

[3] Geosciences Department, University of Wisconsin - Parkside, Kenosha, WI 53141, U.S.A.

[4] Department of Geology, Miami University, Oxford, OH 45056, U.S.A.

*** E-mail:** *hehp@gig.ac.cn*

This is a preprint, the final version is subject to change, of the American Mineralogist (MSA)
Cite as Authors (Year) Title. American Mineralogist, in press.
(DOI will not work until issue is live.) DOI: http://dx.doi.org/10.2138/am-2017-5935

ABSTRACT

Understanding clay mineral transformation is of fundamental importance to unraveling geological and environmental processes, and to better understanding unique structure and property of phyllosilicates. To date, two pathways have been identified, i.e., the transformation among 2:1 type clay minerals (e.g., illitization of smectite) and from 2:1 type to 1:1 type (e.g., kaolinization of smectite). However, the transformation of 1:1 to 2:1 type is less commonly observed. In this study, hydrothermal experiments were conducted to investigate the possibility of the transformation of 1:1 type clay minerals (i.e., halloysite and kaolinite) into 2:1 ones (i.e., beidellite). The obtained products were characterized by XRD, TG, FTIR, ^{27}Al and ^{29}Si MAS NMR, and HRTEM. XRD patterns of the hydrothermal products display characteristic basal spacing of smectite group minerals at 1.2 - 1.3 nm with dramatic decrease/disappearance of the (001) reflection of halloysite and kaolinite. This is consistent with HRTEM observations, in which clay layers with a thickness of 1.2 - 1.4 nm are observed in all hydrothermal products and the Si/Al ratio determined by EDS analysis is close to that of beidellite. The basal spacing increases to approximately 1.70 nm upon ethylene glycolation, displaying swelling ability of the resultant minerals. The consumption of surface OH in precursor minerals during the transformation leads to a dramatic decrease of mass loss of dehydroxylation and merging of the well resolved OH stretching vibrations in precursor minerals into one at ca. 3667 cm^{-1}, which is indicative of beidellite. These results demonstrate that both halloysite and kaolinite can be converted to 2:1 beidellite under hydrothermal

condition, and the transformation of halloysite is easier than that of kaolinite. Such transformation of 1:1 clay minerals to 2:1 ones could be a new pathway for the transformation of clay minerals in nature. Meanwhile, the substitution of Al^{3+} for Si^{4+} is found in all newly formed beidellite, suggesting the chemical composition of the newly formed Si-O tetrahedral sheet is different from the one inherited from the precursor clay minerals. This can well explain the formation of "polar layer" in mixed-layer phyllosilicates. These findings are of high importance for better understanding the transformation among clay minerals and unique structure of mixed-layer phyllosilicates.

Keywords: Clay transformation, hydrothermal condition, halloysite, kaolinite, beidellite

INTRODUCTION

Clay minerals are ubiquitous in the Earth's crust and clay transformations play critical roles in many geologic and environmental processes (e.g., soil formation, diagenesis, clay deposit formation, climate change) (Singer 1980; Christidis and Dunham 1993; Aoudjit et al. 1995; Stern et al. 1997; Wilson 1999). Meanwhile, clay minerals are a family of natural nano-materials with unique structure and chemicophysical nature (Bergaya et al. 2006). Therefore, understanding clay transformation is of fundamental importance to unraveling these processes and to utilizing clay mineral resources.

To date, two pathways have been identified, i.e., the transformation among 2:1 type clay minerals (e.g., illitization of smectite, glauconitization of smectite) (Odin 1988; Stixrude and Peacor 2002) and from 2:1 type to 1:1 type (e.g., kaolinization of smectite) (Altschuler et al. 1963; Ryan and Huertas 2009). Correspondingly, two mechanisms have been proposed to explain these clay transformations: (1) solid-state transformation: conversion from one 2:1 type clay mineral to another in the solid-state by rearrangement of ions within the interlayer as the main route for atom diffusion in and out of the structure (Cuadros and Altaner 1998; Środoń 1999) or stripping off one of the tetrahedral sheets from a 2:1 structure for the transformation from 2:1 to 1:1 type clay minerals (Stixrude and Peacor 2002; Dudek et al. 2006); (2) dissolution-crystallization: dissolution of the original mineral and crystallization of a new mineral (Środoń et al. 2000). The importance of either solid-state or dissolution-crystallization mechanism appears largely controlled by the fluid/rock

ratio (Rozalén et al. 2008).

In comparison to the two above-mentioned transformation pathways, the transformation of 1:1 type clay minerals to 2:1 type ones is less commonly observed. The illitization of kaolinite is mostly reported for the transformation of 1:1 to 2:1 type ones, mainly occurring in diagenesis and low-grade metamorphism (Dunoyer de Segonzac 1970; Sommer 1978; Dutta and Suttner 1986; Lanson et al. 1996, 2002), and under hydrothermal conditions (Šucha et al. 1998; Bentabol et al. 2003, 2003b, 2006). Such transformation strongly depends on temperature, pressure, pH, and K^+/H^+ activity ratio (Huang 1993; Bauer et al. 1998; Mantovani and Becerro 2010; Mantovani et al. 2010), and dissolution-crystallization was proposed to be the main transformation mechanism involved (Chermak and Rimstidt 1990; Bauer et al. 1998; Lanson et al. 2002; Bentabol et al. 2003a, 2006).

As is well known, the basal surface of 1:1 clay minerals is composed of a neutral siloxane surface on the tetrahedral side and a hydroxyl surface on the octahedral side. The siloxane surface is the least reactive on clay minerals while the hydroxyl surface displays high reactivity towards water molecules and other matter in various media (Schoonheydt and Johnston 2013). For example, the surface hydroxyls (e.g., Al-octahedral surface in kaolinite) play a critical role in silylation of clay minerals, in which the surface hydroxyls can condensate with alkoxyl group and/or the hydroxyls in the hydrolyzed silane (Tunney and Detellier 1996; He et al. 2013). Meanwhile, successful syntheses of clay minerals under hydrothermal conditions suggest that chemical bonding of Si-O tetrahedra in solution and octahedral sheet in solid phase is

97 feasible, in which a size match between tetrahedral and octahedral sheets may be a
98 key factor in controlling the formation of clay minerals (He et al. 2014).

99 Accordingly, we hypothesize that a transformation of 1:1 type clay minerals to
100 2:1 type ones can take place in a solid state under hydrothermal conditions. If
101 confirmed, such transformation could be a new pathway for the transformation of clay
102 minerals in nature. Also, such transformation can well explain the formation of the
103 "polar layer" structure in mixed-layer phyllosilicates, in which the two tetrahedral
104 sheets in a TOT unit have different layer charges (McAtee 1958; Dudek et al. 2006).
105 This fundamental work may open up an entirely new avenue for utilizing abundant
106 1:1 clay minerals to synthesize swelling smectite group minerals (e.g., saponite and
107 beidellite), which are less abundant in nature but of higher economic value (Galán and
108 Ferrell 2013).

109 In this study, we conducted hydrothermal experiments to investigate the
110 transformation from 1:1 clay minerals to 2:1 ones, using halloysite and kaolinite as
111 the starting minerals and $Na_2SiO_3 \cdot 9H_2O$ as the source of Si. Our experimental results
112 demonstrate that both halloysite and kaolinite can be transformed into 2:1 type
113 beidellite, in which the morphology of the precursor mineral has a significant effect
114 on the transformation rate. This study provides novel insights for understanding the
115 clay mineral transformation as well as a possible formation mechanism of the "polar
116 layer" structure in mixed-layer phyllosilicates.

117

118 **EXPERIMENTAL METHODS**

Hydrothermal experiments

Two kinds of 1:1 type dioctahedral clay minerals, kaolinite and halloysite, were used as the starting minerals in the transformation experiments. The kaolinite sample of high purity was collected from Maoming, Guangdong Province, China, and was used as collected. The halloysite sample, obtained from Linfen, Shanxi Province, China, was purified by sedimentation and then dried at 120 °C. Their chemical compositions, determined by X-ray fluorescence spectroscopy (XRF), are shown in Table 1. Sodium metasilicate ($Na_2SiO_3 \cdot 9H_2O$) of analytical grade was used as the source of Si.

The hydrothermal experiments were conducted in a stainless steel autoclave at 300 °C under an autogenous water pressure. A general procedure is as follows: 24 g $Na_2SiO_3 \cdot 9H_2O$ were added to 100 mL of deionized water under vigorous stirring. Then, 13.5 mL of hydrochloric acid (*wt*%=36~38%, analytical grade) was slowly added to the obtained solution with continuous stirring, which was used to adjust the pH of the solution to 8. After that, the obtained colloid was transferred to an autoclave, and mixed with 4.4 g halloysite and kaolinite, respectively. The Si/Al ratio in the reaction system was 2:1, close to the stoichiometric ratio for ideal beidellite. The mixture was hydrothermally treated in the autoclave at 300 °C and autogenous water pressure for one to two weeks. In order to exclude the excess electrolytes in the resultant products, the obtained products were washed 6 times with deionized water, then dried at 80 °C, and ground before characterizations. The obtained products were denoted as M-xw, where M = H and K, standing for halloysite and kaolinite,

141 respectively, and xw stands for the duration of the treatment time, i.e., 1w = 1 week
142 and 2w = 2 weeks.

143 **Analytical techniques**

144 **X-ray fluorescence spectroscopy (XRF).** Elemental analysis was conducted on a
145 Rigaku RIX 2000 X-ray fluorescence spectrometer (XRF). Kaolinite and halloysite
146 samples were ground using an agate mortar to 200 mesh. Loss-on-ignition was
147 obtained by weight loss of the sample ignited in a furnace at 900 °C for 2 h and
148 allowed to cool in a desiccator to minimize moisture absorption. About 500 mg
149 calcined samples and 4 g $Li_2B_4O_7$ were mixed homogeneously, and the mixture was
150 digested in a Pt-Au alloy crucible at 1150 ^oC in a high-frequency furnace. The
151 quenched bead was used for XRF measurements. The calibration line for Si/Al ratio
152 used in quantification was produced by bivariate regression of the Si/Al data
153 measured for 36 reference materials encompassing a wide range of silicate
154 compositions, and analytical uncertainties are mostly between 1% and 5%.

155 **X-ray diffraction (XRD).** XRD patterns were collected between 1^o and 65^o (2θ)
156 at a scanning rate of 1^o (2θ) min^{-1} on a Bruker D8 Advance diffractometer with
157 Ni-filtered CuKα radiation (λ=0.154 nm, 40 kV and 40 mA). The oriented samples
158 were prepared by carefully pipetting the clay suspension onto a glass slide and
159 allowing it to dry at ambient temperature. Glycolated samples were prepared by
160 treating the oriented samples in a glass desiccator with ethylene glycol at 30 °C for 24
161 h.

Thermogravimetric analysis (TG). TG analyses were performed on a Netzsch STA 409PC instrument. Approximately 15 mg ground sample was heated in a corundum crucible from 30 to 1000 °C at a heating rate of 10 °C/min under a pure N_2 atmosphere (60 cm^3/min). The differential thermogravimetric (DTG) curve was derived from the TG curve.

Fourier transform infrared spectroscopy (FTIR). The FTIR spectra were obtained on Bruker Vertex-70 Fourier transform infrared spectrometer by using the KBr pressed disk technique. To obtain well-proportioned mixture, each sample was prepared with a clay/KBr ratio of approximate 1:100, and ground in an agate mortar for 10 min. Then the mixture was heated under a lamp for 3 min to minimize water adsorption before FTIR measurements. The spectra were collected over the range of 4000 - 400 cm^{-1} with 64 scans and a resolution of 4 cm^{-1}.

High resolution transmission electron microscopy (HRTEM). HRTEM images were collected on a JEOL 2010 high resolution transmission electron microscope operated at an accelerating voltage of 200 kV. Specimens were prepared by dispersing the samples in ethanol and ultrasonically treating them for 5 minutes. A drop of the resultant suspension was placed on a porous carbon film supported by a copper grid, after which the ethanol was evaporated.

Magic-angle-spinning nuclear magnetic resonance spectroscopy (MAS NMR). ^{27}Al and ^{29}Si MAS NMR experiments were performed on Bruker AVANCE III 600 spectrometer at resonance frequencies of 156.4 and 119.2 MHz, respectively. ^{29}Si MAS NMR spectra with high-power proton decoupling were recorded on a 4 mm

probe with a spinning rate of 12 kHz, a π/4 pulse length of 2.6 μs, and a recycle delay of 80 s. The chemical shifts of ^{29}Si were referenced to tetramethylsilane (TMS). A 4 mm HX double-resonance MAS probe was used to measure ^{27}Al MAS NMR at a sample spinning rate of 14 kHz. The spectra were recorded by a small-flip angle technique with a pulse length of 0.5 μs (< π/12) and a 1s recycle delay. The chemical shift of ^{27}Al was referenced to 1 M aqueous $Al(NO_3)_3$.

RESULTS AND DISCUSSION

Mineralogical characteristics of hydrothermal products

XRD patterns

Both the precursor halloysite and kaolinite display characteristic (001) reflection at 0.72 and 0.71 nm, respectively (Fig. 1). After one week of hydrothermal treatment, the characteristic reflection of halloysite at 0.72 nm disappears; while a broad reflection occurs at approximately 1.24 nm (Fig. 1a). Its intensity increases significantly in the XRD patterns of oriented samples (Fig. 1b). This basal reflection increases to 1.70 nm upon ethylene glycolation (Fig. 1c), suggesting the formation of swelling clay minerals with a 2:1 structure (Suquet et al 1975). After two weeks of treatment, the intensity of the reflection at ca.1.24 nm is further enhanced (Fig. 1a), reflecting an increase of crystallinity as well as the layer stacking order of the newly formed smectite (He et al. 2014). As one of the starting materials is $Na_2SiO_3 \cdot 9H_2O$, the resultant smectite may have Na^+ as its interlayer cation, consistent with the d_{001} of 1.24 nm. To reveal the layer thickness of the dehydrated smectite in the products, the

206 resultant clay mineral was heated at 450 ^{o}C for 1.5 h. A collapse of the interlayer
207 space was observed after heating with a decrease of the basal spacing from 1.24
208 (H-2w) to 0.97 nm (Fig. 2a). This basal spacing of 0.97 nm is identical to that of
209 dehydrated Na-smectite reported in literature (Brindley and Sempels 1977; Ferrage et
210 al. 2007).

211 Similar mineral transformation also takes place for kaolinite during hydrothermal
212 treatment. A new reflection occurs at 1.26 nm, accompanied by a dramatic decrease of
213 the basal reflection intensity of kaolinite at 0.71 nm (Figs. 1d-1f). This reflection
214 increases to 1.68 nm upon ethylene glycolation, corresponding to the swelling ability
215 of the resultant smectite. After heating the hydrothermal products at 450 ^{o}C for 1.5 h,
216 the basal spacing decreases from 1.26 (K-2w) to 0.97 nm (Fig. 2b), identical to that of
217 dehydrated Na-smectite (Brindley and Sempels 1977; Ferrage et al. 2007). However,
218 a weak basal reflection of kaolinite at 0.71 nm is still present in the XRD patterns of
219 the hydrothermal products after one and two weeks. This suggests that kaolinite is
220 more difficult to be transformed into 2:1 type clay minerals than halloysite and the
221 morphology of the precursor clay minerals may have an important effect on the
222 transformation rate.

223 **HRTEM observation**

224 HRTEM observation can provide direct evidences, including changes of layer
225 height and morphology, to reveal the conversion of halloysite and kaolinite to 2:1 type
226 clay minerals. The original halloysite and kaolinite display typical tubular (Fig. 3a)
227 and hexagonal sheet morphology (Fig. 3e) (Alexander et al 1943; Bates et al. 1950),

228 respectively. However, after hydrothermal treatment, clay layers with a thickness of
229 1.2 - 1.4 nm were observed in all hydrothermal products, and the Si/Al ratio
230 determined by EDS analysis is approximately 2:1, close to that of beidellite. In the
231 case of halloysite, HRTEM images revealed that the straight tubes of the original
232 halloysite disappeared after hydrothermal treatment. Clay layers with a thickness of
233 1.2 - 1.3 nm formed along the edges of halloysite tubes where the original halloysite
234 tubes were split apart (Figs. 3b and 3c). Figure 3c clearly shows that the newly formed
235 beidellite can roughly keep its original tubular morphology in the upper part of the
236 tube but is obviously curved, whereas the lower part of the tube was split into two
237 parts. Our measurements show that all these neoformed clay layers have an
238 approximately layer thickness of 1.2 nm, demonstrating that halloysite has been
239 successfully transformed into beidellite.

240 In order to reveal the transformation process of halloysite, HRTEM observation
241 was also conducted on the product of halloysite after 3 days of hydrothermal
242 treatment. The images clearly display mixed layer halloysite-smectite, in which
243 halloysite and the neoformed smectite have a layer thickness of 0.7 and 1.3 nm (Figs.
244 4a and 4c), respectively. However, the halloysite-smectite layer sequences are
245 disordered. More importantly, in a certain layer, the thickness of various parts are
246 obviously different. That is to say, the layer thickness of parts increases to
247 approximately 1.3 nm, attributed to the neoformed smectite, whereas the thickness of
248 other parts remains at 0.7 nm, corresponding to the precursor halloysite (Figs. 4a and
249 4c). These observations strongly suggest that the transformation takes place via a

solid-state conversion.

HRTEM images of kaolinite and its hydrothermal products (Figs. 3e-3g) clearly display the transformation process from kaolinite to beidellite. After hydrothermal treatment, the edges of kaolinite particles become curved, which are composed of layers with a height of approximately 1.2 nm, whereas the central part of kaolinite particle remains unchanged with a flat morphology (Fig. 3f). With an increase of the transformation extent, the whole kaolinite particle was transformed into beidellite accompanied with exfoliation (Fig. 3g). The Si/Al ratio determined by EDS analysis (e.g., the atomic Si/Al ratio for Area A in Fig. 3g is 2.3:1.) is close to that of ideal beidellite. Here, HRTEM images show convincible evidences for the successful transformation from halloysite and kaolinite to beidellite, in which the transformation starts from the edges of precursor minerals.

Thermal Analysis

In 1:1 type clay minerals, the primitive unit cell contains three inner-surface hydroxyls and one inner hydroxyl inside the layer. If the 1:1 type clay minerals can be converted to 2:1 type ones, two-thirds of inner-surface hydroxyls should be replaced by tetrahedral apical oxygen atoms. This may lead to a dramatic decrease of mass loss, corresponding to dehydroxylation. Theoretically, the mass loss of dehydroxylation for kaolinite and halloysite without interlayer water is approximately 14% while that for beidellite is 5% (Malek et al. 1997).

TG curves of halloysite and kaolinite used show that the mass loss of dehydroxylation is 14.4 and 14.1% (Table 2), respectively, which takes place at

around 510 and 528 °C (Fig. 5). Meanwhile, a small amount of mass loss, attributed to adsorbed water in halloysite and kaolinite, was also recorded by TG analyses (Table 2). After hydrothermal treatment with $Na_2SiO_3 \cdot 9H_2O$, the mass loss of dehydroxylation prominently decreases to 3.4% for H-1w, 3.7% for H-2w, 5.5% for K-1w and 5.3% for K-2w, respectively. However, our contrast experiments demonstrate that hydrothermal treatment under identical conditions but without $Na_2SiO_3 \cdot 9H_2O$ could lead to a slight decrease of the mass loss of dehydroxylation (Figs. 5b and 5f), but it is much less than the prominent decrease as observed in the hydrothermal products treated with $Na_2SiO_3 \cdot 9H_2O$ (Table 2). This implies a successful transformation of 1:1 type clay minerals to 2:1 type ones, in which inner-surface hydroxyls in precursor minerals were consumed and resulted in a dramatic mass loss decrease of dehydroxylation for the resultant beidellite. Due to the poor crystallinity, the dehydroxylation temperature of the newly formed beidellite occurs at approximately 480 and 510 °C (Fig. 5), respectively, obviously lower than that of the precursor halloysite and kaolinite. Meanwhile, a prominent mass loss at low temperature range (room temperature to ca. 300 °C) (Table 2), corresponding to the losses of the adsorbed water and coordinated water associated with the interlayer cations in neoformed beidellite, was recorded in TG curves of the hydrothermal products (Figs. 5c, 5d, 5g and 5h). It is noteworthy that, since 7Å-halloysite was used in the hydrothermal experiments, the loss of interlayer water of halloysite does not contribute at this temperature range. The prominent increase of mass loss at this low temperature range should be attributed to the coordinated water associated with the

interlayer Na^+ in the newly formed beidellite, reflecting the successful transformation of halloysite and kaolinite into beidellite.

FTIR spectra

Provided that 1:1 type clay minerals can transform into 2:1 type ones in the solid state, a critical step is the attachment of a Si-O tetrahedral sheet to the 1:1 layer of precursor mineral. In this procedure, condensation between the surface OH of the precursor mineral and the silanols in Si source (e.g., individual or polymers of Si-O tetrahedra with OH resulted from hydrolysis of sodium metasilicate in this study) will take place. This will lead to consumption of surface hydroxyls in precursor minerals, and subsequently, significant changes of hydroxyl stretching vibration modes. In this study, FTIR spectra show a prominent decrease of both the intensity and resolution of the structural hydroxyl stretching vibrations at 3600 - 3700 cm^{-1} with an extension of hydrothermal reaction duration (Fig. 6), indicating consumption of surface hydroxyls during the transformation. For instance, the original halloysite displays two well-resolved stretching vibration bands at 3622 and 3697 cm^{-1} (Fig. 6a), corresponding to inner OH and inner-surface OH (Kloprogge and Frost 2000; Madejova and Komadel 2001), respectively. After hydrothermal treatment, the two vibrations merge to one at ca. 3667 cm^{-1}, which is indicative of the structural OH stretching vibration in beidellite (Russell 1987).

Similar FTIR spectral evolution was also found for kaolinite (Figs. 6d-6f) before and after hydrothermal treatments. Four well resolved OH stretching vibrations at 3695 (strong), 3668 (weak), 3654 (weak) and 3621 (strong) cm^{-1}, were recorded, of

316 which the former three vibrations correspond to inner-surface OH and the one at 3621
317 cm^{-1} is attributed to inner OH (Madejova and Komadel 2001). After one week's
318 treatment, the FTIR spectrum of K-1w displays only three OH stretching vibrations at
319 3696, 3650 and 3621 cm^{-1}, respectively, with dramatic decreases in intensity and
320 resolution. Simultaneously, the vibration at 914 cm^{-1}, due to the bending vibration of
321 inner hydroxyl of kaolinite (Madejova and Komadel 2001), is still visible. This
322 reflects the presence of kaolinite remnant in the hydrothermal product as revealed by
323 both XRD patterns and HRTEM images, i.e., the products are composed of kaolinite
324 remnant and newly formed beidellite. With an extension of hydrothermal treatment
325 duration, the three stretching vibrations of inner surface OH merge to one at
326 approximately 3650 cm^{-1}, indicative of the hydroxyl stretching vibration in beidellite
327 (Russell 1987), and the intensity of inner OH stretching vibration at 3620 cm^{-1}
328 significantly decreases but is still distinguishable. This strongly suggests that the
329 transformation of kaolinite into beidellite is more difficult than halloysite, consistent
330 with the conclusion made from the XRD patterns and HRTEM images. Here, all the
331 characterization results suggested the successful transformation of halloysite and
332 kaolinite into beidellite under hydrothermal condition.

333 **MAS NMR spectra**

334 In ^{27}Al MAS NMR spectra of halloysite (Fig. 7a) and kaolinite (Fig. 7b), only
335 one signal at ca. 6.8 ppm was recorded, corresponding to 6-coordinated Al (Al(VI)) in
336 the octahedral sheets (He et al. 2003). However, two 4-coordinated Al (Al(IV))
337 signals at ca. 71 and 55 ppm were recorded in ^{27}Al MAS NMR spectra of the

hydrothermal products, in addition to the dominant signal of Al(VI) at ca. 6 ppm. The Al(IV) signal at ca. 71 ppm is due to the substitution of Al^{3+} for Si^{4+} in tetrahedral sheets while the one at ca. 55 ppm corresponds to Al in the three-dimensional silica framework (Breen et al. 1995), where the latter was formed by polymerization of metasilicate. The assignments of the Al(IV) signals were further evidenced by ^{29}Si NMR spectra. Both ^{29}Si MAS NMR spectra of the precursor halloysite and kaolinite display a single signal at approximately -91 ppm (Figs. 7c and 7d), corresponding to $Q^3(0Al)$ (Rocha and Klinowski 1990; He et al. 2003). However, in ^{29}Si spectra of the hydrothermal products, two poorly resolved $Q^3(0Al)$ and $Q^3(1Al)$ signals occur at -90 ~ -92 and ca. -87 ppm, respectively, corresponding to the newly formed beidellite, while a broad Q^4 signal was recorded at ca. -106 ppm (Figs. 7c and 7d), attributed to three-dimensional silica (Altaner et al. 1988; Stucki 1996). The occurrence of two different Al(IV) signals, $Q^3(0Al)$ and $Q^3(1Al)$, suggests that the chemical composition of the newly formed Si-O tetrahedral sheet is different from the one inherited from the precursor clay minerals. In other words, the inherited Si-O tetrahedral sheet is identical to that in halloysite and kaolinite without isomorphous substitution, corresponding to $Q^3(0Al)$; while the newly formed Si-O tetrahedral sheet contains the substitution of Al^{3+} for Si^{4+}, corresponding to $Q^3(1Al)$. This leads to coexistence of the two tetrahedral sheets with different charge and chemical composition in a TOT unit. Our study demonstrates that the substitution of Al^{3+} for Si^{4+} in the tetrahedral sheets is not only beneficial for the formation of smectite minerals, which can improve the size matching between octahedral and tetrahedral sheets (He et al. 2014),

but also develops the layer charge required to form smectite minerals under hydrothermal conditions. More importantly, such transformation from 1:1 to 2: 1 layer type by the mechanism described above may explain the origin of polar layer structure in phyllosilicates. The newly formed tetrahedral sheet is rich in the substitution of Al^{3+} for Si^{4+}, resulting in higher layer charge than the original one which is inherited from the precursor mineral and poor in isomorphous substitution. Thus, layer charge for the two tetrahedral sheets in the same TOT unit is different. Consequently, polar layer is formed in phyllosilicates (Sudo et al. 1962; Cuadros and Linares 1995).

Transformation mechanism

To elucidate the transformation mechanism, dissolution experiments of halloysite and kaolinite were conducted under identical conditions as hydrothermal transformation experiments but without adding $Na_2SiO_3 \cdot 9H_2O$. The identical XRD patterns and FTIR spectra of halloysite and kaolinite before and after hydrothermal treatment without $Na_2SiO_3 \cdot 9H_2O$ (not shown) suggest that these precursor minerals are relatively stable in the absence of Si and Na. It is noteworthy that TG analyses of halloysite and kaolinite samples after dissolution experiment display a slight decrease of mass loss corresponding to dehydroxylation (Figs. 5b and 5f, and Table 2), in comparison to that of the precursor halloysite and kaolinite. This should be attributed to the consumption of surface hydroxyls, resulted from the reaction between surface hydroxyls and OH^- in the mildly alkaline solution. Such surface hydroxyl consumption can well explain the decreased mass loss of dehydroxylation for the newly formed beidellite from halloysite (Table 2), in comparison to the theoretical

382 value of beidellite (approximately 5%). That is to say, more than two-thirds of surface
383 hydroxyls in halloysite are consumed during the transformation, through the
384 condensation between inner-surface hydroxyls and hydrolyzed metasilicate, and the
385 reaction between surface hydroxyls and OH^- in the mildly alkaline solution.

386 Meanwhile, HRTEM observations show that the surfaces of both hydrothermally
387 treated halloysite and kaolinite (without $Na_2SiO_3 \cdot 9H_2O$) are slightly obscure (Figs. 3d
388 and 3h) when compared with that before hydrothermal treatment (Figs. 3a and 3e).
389 This implies the occurrence of limited dissolution, mainly on outer surfaces and
390 broken edge sites (Ramos et al. 2014), despite our measurements show that the
391 concentration of the dissolved Al in the supernatant solution is as low as 1-2 ppb. This
392 was also evidenced by ^{27}Al MAS NMR spectra of the hydrothermal products. In the
393 reaction systems, halloysite or kaolinite is the only phase containing Al, which occupy
394 the octahedral sites in mineral structure. The occurrence of Al in the tetrahedral sheet
395 of the newly formed smectite and amorphous silica in the hydrothermal products
396 strongly suggests limited dissolution in the transformation process. However, such
397 limited dissolution is beneficial for the transformation and development of the layer
398 charge in the resultant smectite. Our recent study (He et al. 2014) demonstrates that
399 the substitution of Al^{3+} for Si^{4+} in the tetrahedral sheets is beneficial for the formation
400 of smectite minerals under hydrothermal condition, which may improve the size
401 matching between octahedral and tetrahedral sheets.

402 In this study, the HRTEM images of kaolinite, halloysite and their hydrothermal
403 products provide clear evidences for the transformation procedure. The precursor

404 kaolinite displays typically hexagonal sheet morphology (Fig. 3e). After hydrothermal
405 treatment, part of kaolinite particle edges obviously becomes curved (Fig. 3f), which
406 is composed of layers with a thickness of approximately 1.2 nm and an atomic ratio of
407 Si/Al close to that of beidellite. However, other parts of the kaolinite particle remain a
408 flat morphology as that of the precursor kaolinite. This implies no transformation in
409 these corresponding parts. EDS analyses of these unreacted parts show a higher Si/Al
410 ratio (not shown) in comparison to the theoretical value of kaolinite. This should be
411 attributed to the precipitation of amorphous SiO_2 (polymerized metasilicate) on the
412 mineral surface as indicated by XRD patterns and ^{29}Si MAS NMR spectra of the
413 hydrothermal products. With an extension of reaction time, very few precursor
414 kaolinite particles can be found in the hydrothermal products. Instead, curved and
415 exfoliated layers with a thickness of 1.1 - 1.4 nm and similar chemical composition as
416 that of beidellite can be observed extensively. The ethylene glycolation experiments
417 demonstrate that these resulting minerals have excellent swelling ability.

418 In the case of halloysite, the HRTEM images of the products of halloysite after 3
419 days of hydrothermal treatment clearly display mixed-layer structure with disordered
420 stacking of halloysite and smectite layers (Figs. 4a and 4c). Our observation is very
421 similar to that for kaolinization of smectite reported by Amouric and Olives (1996),
422 but in reverse order. This implies that the transformation between kaolinite and
423 smectite is reversible and controlled by physicochemical conditions of the reaction
424 system.

425 The obtained results illuminate the successful transformation of kaolinite and

426 halloysite into beidellite, which starts from the edges of precursor minerals (Fig. 8). In
427 the transformation process, individual or polymers of Si-O tetrahedra may act as
428 'wedges' to intercalate into the interlayer space. Then they could attach to the
429 octahedral sheet of 1:1 clay minerals via condensation between the intercalated Si-O
430 tetrahedra and inner-surface hydroxyls of precursor clay minerals (He et al. 2014).
431 This condensation reaction was evidenced by both the dramatic mass loss decrease of
432 dehydroxylation in the resultant products (Fig. 5) and the evolution of the OH
433 stretching vibrations at 3600 - 3700 cm^{-1} (Fig. 6). Due to the intercalation of Si-O
434 tetrahedra, exfoliation may take place during the transformation as revealed by
435 HRTEM images. Depending on the orientation of the re-assembly of individual 2:1
436 layers, different structures may form (Fig. 8).
437
438 **IMPLICATIONS**
439 Our results demonstrate a transformation mechanism from 1:1 type clay minerals
440 to 2:1 type ones in solid state under hydrothermal condition, which might be a new
441 pathway for the transformation of clay minerals in nature.
442 Both ^{27}Al and ^{29}Si MAS NMR spectra of the hydrothermal treatment products
443 can reveal the occurrence of the substitution of Al^{3+} for Si^{4+} in the newly formed Si-O
444 tetrahedral sheets of the resultant beidellite. These results imply that the substitution
445 of Al^{3+} for Si^{4+} is critical for the transformation reaction, and may improve the size
446 matching between the octahedral sheet of the precursor mineral and the newly formed
447 tetrahedral sheet (He et al. 2014). But such substitution results in chemical

448 composition and layer charge differences between the original and the newly formed
449 tetrahedral sheets. Such a transformation mechanism can well explain the "polar layer"
450 structure in mixed-layer phyllosilicates, i.e., the two tetrahedral sheets across the
451 octahedral sheet have different chemical compositions and layer charges.

452 Our results also illuminate that a transformation of 1:1 type clay minerals to 2:1
453 type ones is feasible under hydrothermal condition with mildly alkaline pH and
454 enrichment of Si. From the point of energy, breaking a chemical bond (e.g., Si-O-Si in
455 tetrahedral sheet and Si-O-Al at the crystal edge) (Dudek et al. 2006; Rozalén et al.
456 2008) needs high energy, while condensation between Si-O tetrahedra and surface
457 hydroxyls of precursor clay minerals can decrease the energy of reaction system. That
458 is to say, a transformation of 1:1 to 2:1 type clay minerals (we call it "smectization of
459 1:1 type clay minerals".) is more feasible than that of 2:1 to 1:1 type clay (e.g.,
460 kaolinization of smectite). Hence, our findings provide new-sight to understand the
461 formation mechanism of 2:1 type clay minerals and the genesis of clay deposits such
462 as bentonite.

463

464 **ACKNOWLEDGEMENTS**

465 This work was financially supported by National Natural Science Foundation of
466 China (Grant Nos. 41530313, 41372048), CAS Key Research Program of Frontier
467 Sciences (Grant No. QYZDJ-SSW-DQC023-1) and the CAS/SAFEA International
468 Partnership Program for Creative Research Teams (Grant No. 20140491534).

469

REFERENCES CITES

Alexander, L.T., Faust, G.T., and Hendricks, S.B. (1943) Relationship of the clay minerals halloysite and endellite. American Mineralogist, 28, 1-18.

Altaner, S.P., Weiss, C.A., and Kirkpatrick, R.J. (1988) Evidence from ^{29}Si NMR for the structure of mixed-layer illite/smectite clay minerals. Nature, 331, 699-702.

Altschuler, Z.S., Dwornik, E.J., and Kramer, H. (1963) Transformation of montmorillonite to kaolinite during weathering. Science, 141, 148-152.

Aoudjit, H., Robert, M., Elsass, F., and Curmi, P. (1995) Detailed study of smectite genesis in granitic saprolites by analytical electron microscopy. Clay Minerals, 30, 135-148.

Bates, T.F., Hildebrand, F.A., and Swineford, A. (1950) Morphology and structure of endellite and halloysite. American Mineralogist, 35, 463-484.

Bauer, A., Velde, B., and Berger, G. (1998) Kaolinite transformation in high molar KOH solutions. Applied Geochemistry, 13, 619-629.

Bentabol, M., Cruz, M.D.R., Huertas, F.J., and Linares, J. (2003) Hydrothermal transformation of kaolinite to illite at 200 and 300 ^{o}C. Clay Minerals, 38, 161-172.

——— (2003) Characterization of the expandable clays formed from kaolinite at 200 ^{o}C. Clay minerals, 38, 445-458.

——— (2006) Chemical and structural variability of illitic phases formed from kaolinite in hydrothermal conditions. Applied Clay Science, 32, 111-124.

492 Bergaya, F., Theng, B.K.G., and Lagaly, G. (2006) Clays in industry. In F. Bergaya,
493 B.K.G. Theng and G. Lagaly, Eds., Handbook of Clay Science, p. 499-622.
494 Elsevier, Kidlington, Oxford.
495 Breen, C., Madejová, J., and Komadel, P. (1995) Correlation of catalytic activity with
496 infra-red, ^{29}Si MAS NMR and acidity data for HCl-treated fine fractions of
497 montmorillonites. Applied Clay Science, 10, 219-230.
498 Chermak, J.A., and Rimstidt, J.D. (1990) The hydrothermal transformation rate of
499 kaolinite to muscovite/illite. Geochimica et Cosmochimica Acta, 54,
500 2979-2990.
501 Christidis, G., and Dunham, A.C. (1993) Compositional variation in smectites: Part I.
502 Alteration of intermediate volcanic rocks. Acase study from Milos Island,
503 Greece. Clay Minerals, 28, 255-274.
504 Cuadros, J., and Linares, J. (1995) Some evidence supporting the existence of polar
505 layers in mixed-layer illite/smectite. Clays and Clay minerals, 43, 467-473.
506 Cuadros, J., and Altaner, S.P. (1998) Characterization of mixed-layer illite-smectite
507 from bentonites using microscopic, chemical, and X-ray methods: Constraints
508 on the smectite-to-illite transformation mechanism. American Mineralogist, 83,
509 762-774.
510 Dudek, T., Cuadros, J., and Fiore, S. (2006) Interstratified kaolinite-smectite: Nature
511 of the layers and mechanism of smectite kaolinization. American Mineralogist,
512 91, 159-170.
513 Dunoyer de Segonzac, G. (1970) The transformation of clay minerals during

514 diagenesis and low-grade metamorphism: a review. Sedimentology, 15,
515 281-346.
516 Dutta, P.K., and Suttner, L.J. (1986) Alluvial sandstone composition and paleoclimate,
517 II. Authigenic mineralogy. Journal of Sedimentary Petrology, 56, 346-358.
518 Ferrage, E., Lanson, B., Sakharov, B.A., Geoffroy, N. Jacquot, E., and Drits, V.A.
519 (2007) Investigation of dioctahedral smectitie hydration properties by
520 modeling of X-ray diffracion profiles: Influence of layer charge and charge
521 location. American mineralogist, 92, 1731-1743.
522 Galán, E., and Ferrell, R.E. (2013) Genesis of clay minerals. In F. Bergaya and G.
523 Lagaly, Eds., Handbook of Clay Science, p. 83-126. Elsevier, Kidlington,
524 Oxford.
525 He, H.P., Guo, J.G., Zhu, J.X., and Hu, C. (2003) ^{29}Si and ^{27}Al MAS NMR study of
526 the thermal transformations of kaolinite from North China. Clay Minerals, 38,
527 551-559.
528 He, H.P., Tao, Q., Zhu, J.X., Yuan, P., Shen, W., and Yang, S.Q. (2013) Silylation of
529 clay mineral surfaces. Applied Clay Science, 71, 15-20.
530 He, H.P., Li, T., Tao, Q., Chen, T.H., Zhang, D., Zhu, J.X., Yuan, P., and Zhu, R.L.
531 (2014) Aluminum ion occupancy in the structure of synthetic saponites: Effect
532 on crystallinity. American Mineralogist, 99, 109-116.
533 Huang, W.-L. (1993) The formation of illitic clays from kaolinite in KOH solution
534 from 225 ^{o}C to 350 ^{o}C. Clays and Clay minerals, 41, 645-654.
535 Kloprogge, J.T., and Frost, R.L. (2000) The effect of synthesis temperature on the

FT-Raman and FT-IR spectra of saponites. Vibrational Spectroscopy, 23, 119-127.

Lanson, B., Beaufort, D., Berger, G., Baradat, J., and Lacharpagen, J.-C. (1996) Illitization of diagenetic kaolinite-to-dickite conversion series: Late-stage diagenesis of the Lower Permian Potliegend sandstone reservoir, offshore of the Netherlands. Journal of Sedimentary Researh, Section A: Sedimentary Petrology and Processes, 66, 501-518.

Lanson, B., Beaufort, D., Berger, G., Bauer, A., Cassagnabère, A., and Meunier, A. (2002) Authigenic kaolin and illitic minerals during burial diagenesis of sandstones: a review. Clay Minerals, 37, 1-22.

Madejova, J., and Komadel, P. (2001) Baseline studies of the clay minerals society source clays: infrared methods. Clays and clay minerals, 49, 410-432.

Malek, Z., Balek, V., Garfinke-Shweky, D., and Yariv, S. (1997) The study of the dehydration and dehydroxylation of smectites by emanation thermal analysis. Journal of Thermal Analysis, 48, 83-92.

Mantovani, M., Escudero, A., and Becerro, A.I. (2010) Effect of pressure on kaolinite illitization. Applied Clay Science, 50, 342-347.

Mantovani, M., and Becerro, A.I. (2010) Illitization of kaolinite: The effect of pressure on the reaction rate. Clays and Clay Minerals, 58, 766-771.

McAtee, J.L. (1958) Heterogeneity in montmorillonite. Clays and Clay Minerals, 5, 279-288.

Odin, G.S. (1988) Glaucony from the Gulf of Guinea. In G.S. Odin, Ed., Green

Marine Clays: Oolitic Ironstone Facies, Verdine Facies, Glaucony Facies and Celadonite-Bearing Facies - A Comparative Study, p. 225-248, Elsevier, Amsterdam.

Ramos, M.E., Garcia-Palma, S., Rozalen, M., Johnston, C.T., and Huertas, F.J. (2014) Kinetics of montmorillonite dissolution: An experimental study of the effect of oxalate. Chemical Geology, 363, 283-292.

Rocha, J., and Klinowski, J. (1990) ^{29}Si and ^{27}Al magic-angle-spinning NMR studies of the thermal transformation of kaolinite. Physics and Chemistry of Minerals, 17, 179-186.

Rozalén, M.L., Huertas, F.J., Brady, P.V., Cama, J., García-Palma, S., and Linares, J. (2008) Experimental study of the effect of pH on the kinetics of montmorillonite dissolution at 25 ^{o}C. Geochimica et Cosmochimica Acta, 72, 4224-4253.

Russell, J.D. (1987) Infrared methods. In M.J. Wilson, Ed., A Hand book of Determinative Methods in Clay Mineralogy, p. 133-173. Blackie, Glasgow and London.

Ryan, P.C, and Huertas, F.J. (2009) The temporal evolution of pedogenic Fe-smectite to Fe-kaolin via interstratified kaolin-smectite in a moist tropical soil chronosequence. Geoderma, 151, 1-15.

Schoonheydt, R.A., and Johnston, C.T. (2013) Surface and interface chemistry of clay minerals. In F. Bergaya and G. Lagaly, Eds., Handbook of Clay Science, p. 142-148. Elsevier, Kidlington, Oxford.

580 Singer, A. (1980) The paleoclimatic interpretation of clay minerals in soils and
581 weathering profiles. Earth-Science Reviews, 15, 303-326.
582 Sommer, F. (1978) Diagenesis of Jurassic sandstones in the Viking Graben. Journal of
583 the Geological Society, 135, 63-67.
584 Środoń, J. (1999) Nature of mixed-layer clays and mechanisms of their formation and
585 alteration. Annual Review of Earth and Planetary Sciences, 27, 19-53.
586 Środoń, J., Eberl, D.D., and Drits, V.A. (2000) Evolution of fundamental-particle size
587 during illitization of smectite and implications for reaction mechanism. Clays
588 and Clay Minerals, 48, 446-458.
589 Stern, L.A., Chamberlain, C.P., Reynolds, R.C., and Johnson, D.G. (1997) Oxygen
590 isotope evidence of climate change from pedogenic clay minerals in the
591 Himalayan molasse. Geochimica et Cosmochimica Acta, 61, 731-744.
592 Stixrude, L., and Peacor, D.R. (2002) First-principles study of illite-smectite and
593 implications for clay mineral systems. Nature, 420, 165-168.
594 Stucki, J.W. (1996) Dissolution of hectorite in inorganic acids. Clays and Clay
595 Minerals, 44, 228-236.
596 Šucha, V., Elsass, F., Eberl, D.D., Kuchta, L., Madejová, J., Gates, W.P., and
597 Komadel, P. (1998) Hydrothermal synthesis of ammonium illite. American
598 Mineralogist, 83, 58-67.
599 Suquet, H., de la Calle, C., and Pezerat, H. (1975) Swelling and structural
600 organization of saponite. Clays and Clay Minerals, 23, 1-9.
601 Tunney, J.J., and Detellier, C. (1996) Chemically modified kaolinite. Grafting of

602 methoxy groups on the interlamellar aluminol surface of kaolinite. Journal of
603 Materials Chemistry, 6, 1679-1685.
604 Wilson, M.J. (1999) The origin and formation of clay minerals in soils: past, present
605 and future perspectives. Clay Minerals, 34, 7-25.

606

FIGURE CAPTIONS

Figure 1. XRD patterns of halloysite, kaolinite and their hydrothermal products with $Na_2SiO_3 \cdot 9H_2O$. **(a)** Randomly oriented halloysite (H) and its hydrothermal products (H-1w and H-2w). **(b)** Oriented halloysite (H-O) and its hydrothermal products (H-1w-O and H-2w-O). **(c)** Glycolated halloysite (H-G) and its hydrothermal products (H-1w-G and H-2w-G). **(d-f)** Randomly oriented, oriented, and glycolated samples of kaolinite (K) and its hydrothermal products. (O = oriented sample, G = glycolated sample)

Figure 2. XRD patterns of the hydrothermal products of halloysite (a) and kaolinite (b) and the corresponding samples heated at 450 ^{o}C for 1.5 h.

Figure 3. HRTEM images of halloysite, kaolinite and their hydrothermally treated products. **(a)** The original halloysite. **(b,c)** Hydrothermally treated products of halloysite with $Na_2SiO_3 \cdot 9H_2O$ after one and two weeks. **(d)** Halloysite after two weeks' dissolution experiment without $Na_2SiO_3 \cdot 9H_2O$ (H-D-2w). **(e)** The original kaolinite. **(f)** Hydrothermally treated product of kaolinite with $Na_2SiO_3 \cdot 9H_2O$ after one week. The parts marked with square became curved, which are composed of beidellite layers. **(g)** Hydrothermally treated product of kaolinite with $Na_2SiO_3 \cdot 9H_2O$ after two weeks, beidellite layers with a thickness of 1.2-1.4 nm were extensively formed accompanied with exfoliation. **(h)** Kaolinite after two weeks' dissolution experiment without $Na_2SiO_3 \cdot 9H_2O$ (K-D-2w).

629 **Figure 4.** HRTEM images of the products of halloysite after 3 days of hydrothermal
630 treatment. H = halloysite layer (0.7 nm thick); S = smectite layer (1.3 nm thick). The
631 lateral transition H → S is indicated by arrows.

632

633 **Figure 5.** TG and DTG curves of halloysite, kaolinite, and their hydrothermally
634 treated products. **(a,c,d)** Halloysite (H) and its hydrothermal products with
635 $Na_2SiO_3 \cdot 9H_2O$ after one week (H-1w) and two weeks (H-2w). **(b)** Halloysite after two
636 weeks' dissolution experiment without $Na_2SiO_3 \cdot 9H_2O$ (H-D-2w). **(e,g,h)** Kaolinite (K)
637 and its hydrothermal products with $Na_2SiO_3 \cdot 9H_2O$ after one week (K-1w) and two
638 weeks (K-2w). **(f)** Kaolinite after two weeks' dissolution experiment without
639 $Na_2SiO_3 \cdot 9H_2O$ (K-D-2w).

640

641 **Figure 6.** FTIR spectra of halloysite, kaolinite and their hydrothermal products. **(a-c)**
642 Halloysite (H), and its products after one week (H-1w) and two weeks (H-2w) of
643 hydrothermal treatment. **(d-f)** Kaolinite (K), and its products after one week (K-1w)
644 and two weeks (K-2w) of hydrothermal treatment.

645

646 **Figure 7.** ^{27}Al (left) and ^{29}Si (right) MAS NMR spectra of halloysite, kaolinite, and
647 their hydrothermal products. **(a,c)** Halloysite (H) and the products after one week
648 (H-1w) and two weeks (H-2w) of hydrothermal treatment. **(b,d)** Kaolinite (K) and the
649 products after one week (K-1w) and two weeks (K-2w) of hydrothermal treatment.

650

651 **Figure 8.** Schematic representation of the transformation from 1:1 type clay minerals
652 to 2:1 ones. **(a)** The newly formed tetrahedral sheet is attached to the pre-existing 1:1
653 unit from the same direction. **(b)** The two newly formed tetrahedral sheets are
654 attached from two opposite direction, forming a symmetry across the interlayer, which
655 is a typical mixed layer structure with “polar layers”.
656

657

658 **Table 1.** The chemical compositions of kaolinite and halloysite

659

	Al_2O_3	CaO	Fe_2O_3	K_2O	MgO	Na_2O	SiO_2	TiO_2	H_2O	Total (%)
Kaolinite	36.95	0.10	0.73	0.58	0.15	0.04	46.59	0.32	13.39	98.95
Halloysite	38.21	0.47	0.06	-	-	-	44.92	-	14.95	98.61

660

661

This is a preprint, the final version is subject to change, of the American Mineralogist (MSA)
Cite as Authors (Year) Title. American Mineralogist, in press.
(DOI will not work until issue is live.) DOI: http://dx.doi.org/10.2138/am-2017-5935

662

663 **Table 2**. The mass losses of samples at different temperature ranges (*wt*%).

664

	samples	dehydration (30 - 300 °C)	dehydroxylation (300 - 800 °C)
Halloysite (H)	H	1.5	14.4
	H-1w	7.0	3.4
	H-2w	6.7	3.7
	H-D-1w	0.9	12.1
	H-D-2w	0.8	12.5
Kaolinite (K)	K	2.0	14.1
	K-1w	4.4	5.5
	K-2w	3.2	5.3
	K-D-1w	1.8	13.7
	K-D-2w	0.7	12.2

665 Note: H-D-1w and H-D-2w mean that halloysite was hydrothermally treated for one
666 week and two weeks, respectively, under identical conditions as the transformation
667 experiment but without $Na_2SiO_3 \cdot 9H_2O$. K-D-1w and K-D-2w were denoted as the
668 same way.

This is a preprint, the final version is subject to change, of the American Mineralogist (MSA)
Cite as Authors (Year) Title. American Mineralogist, in press.
(DOI will not work until issue is live.) DOI: http://dx.doi.org/10.2138/am-2017-5935

Figure 1

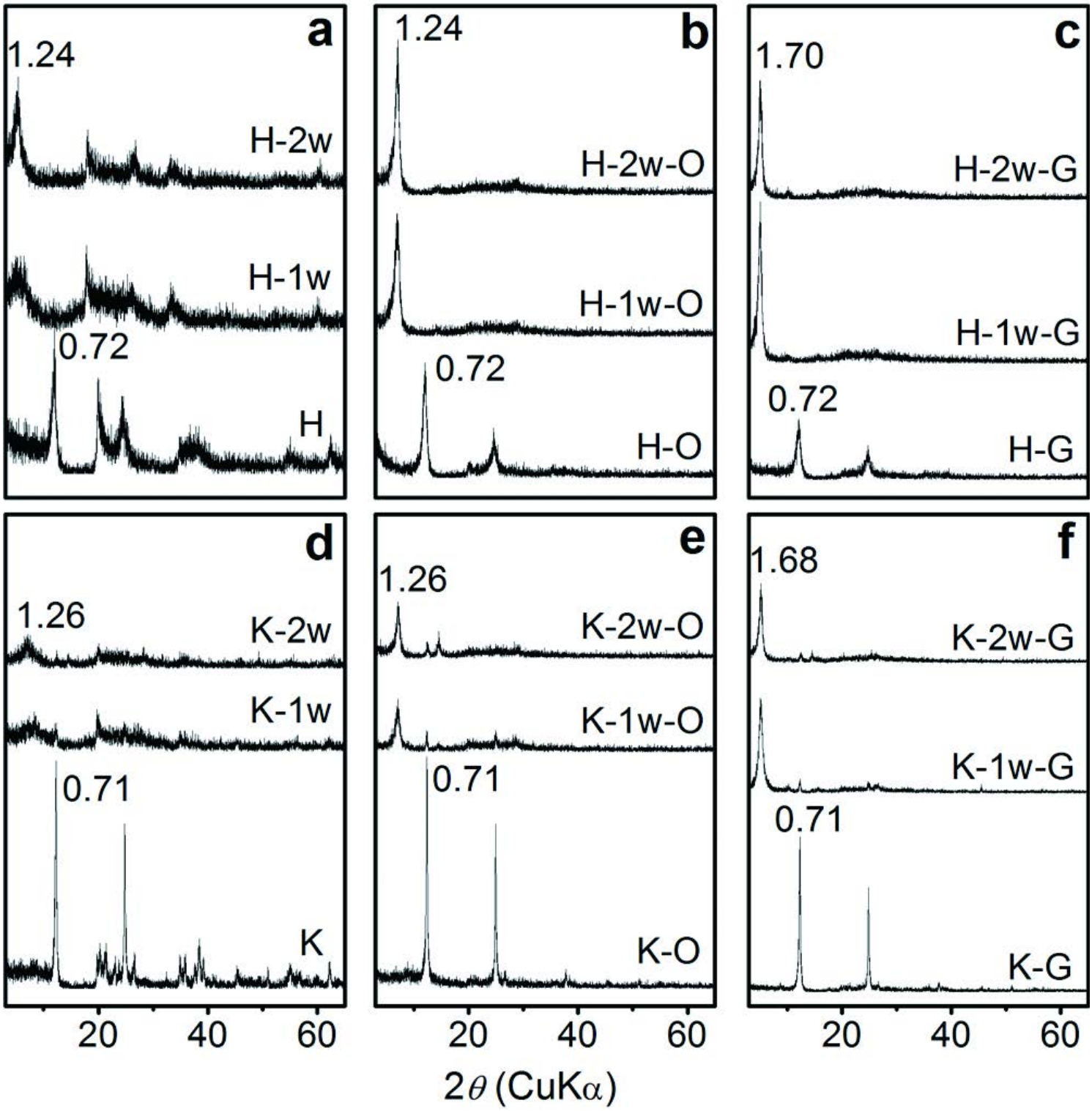

This is a preprint, the final version is subject to change, of the American Mineralogist (MSA)
Cite as Authors (Year) Title. American Mineralogist, in press.
(DOI will not work until issue is live.) DOI: http://dx.doi.org/10.2138/am-2017-5935

Figure 2

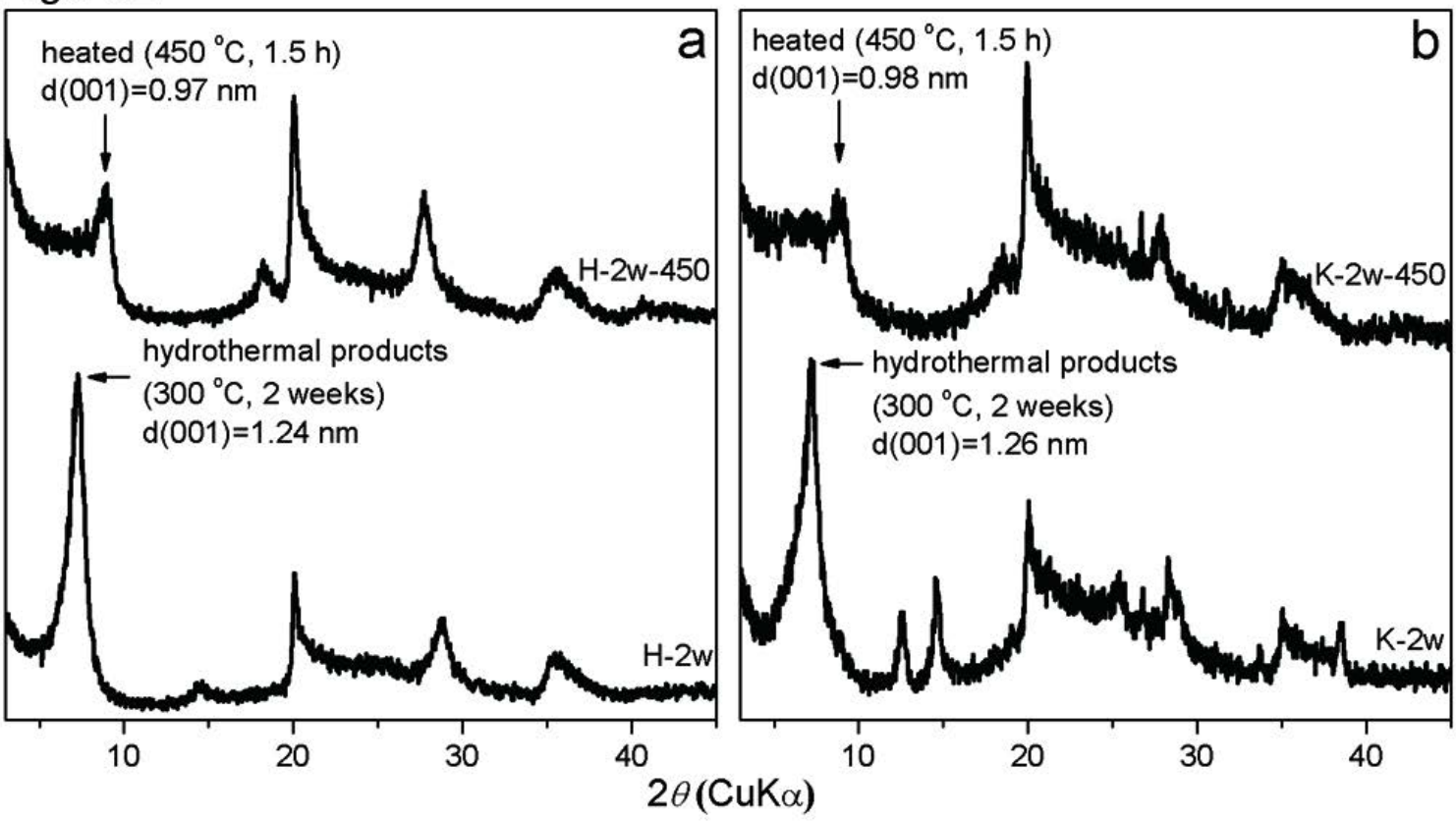

This is a preprint, the final version is subject to change, of the American Mineralogist (MSA)
Cite as Authors (Year) Title. American Mineralogist, in press.
(DOI will not work until issue is live.) DOI: http://dx.doi.org/10.2138/am-2017-5935

Figure 3

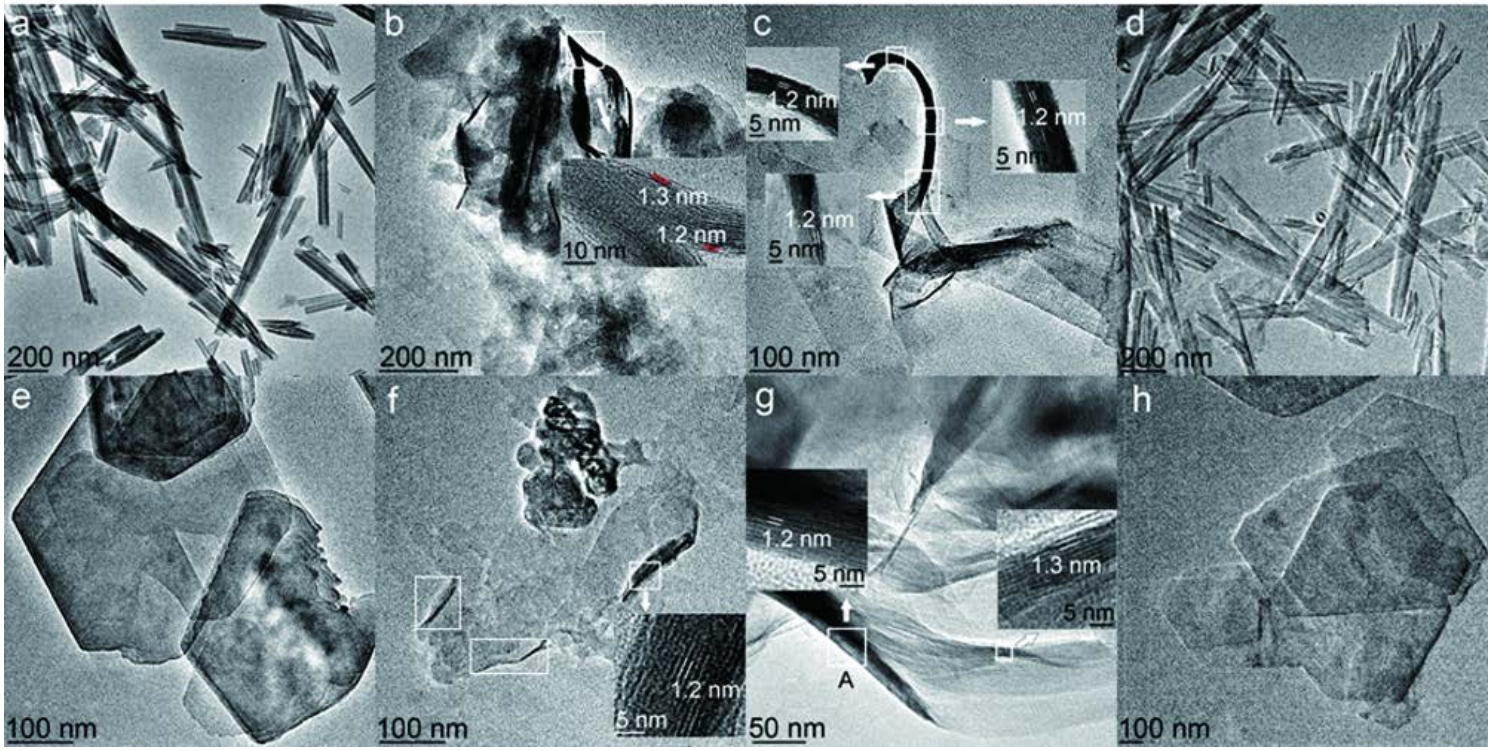

This is a preprint, the final version is subject to change, of the American Mineralogist (MSA)
Cite as Authors (Year) Title. American Mineralogist, in press.
(DOI will not work until issue is live.) DOI: http://dx.doi.org/10.2138/am-2017-5935

Figure 4

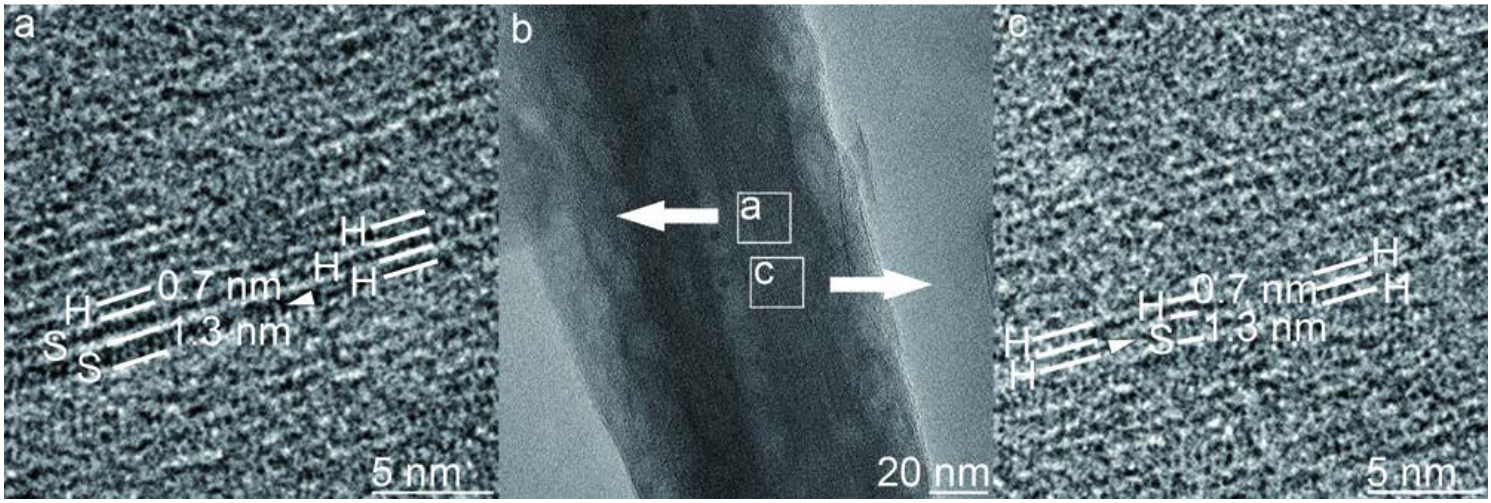

This is a preprint, the final version is subject to change, of the American Mineralogist (MSA)
Cite as Authors (Year) Title. American Mineralogist, in press.
(DOI will not work until issue is live.) DOI: http://dx.doi.org/10.2138/am-2017-5935

Figure 5

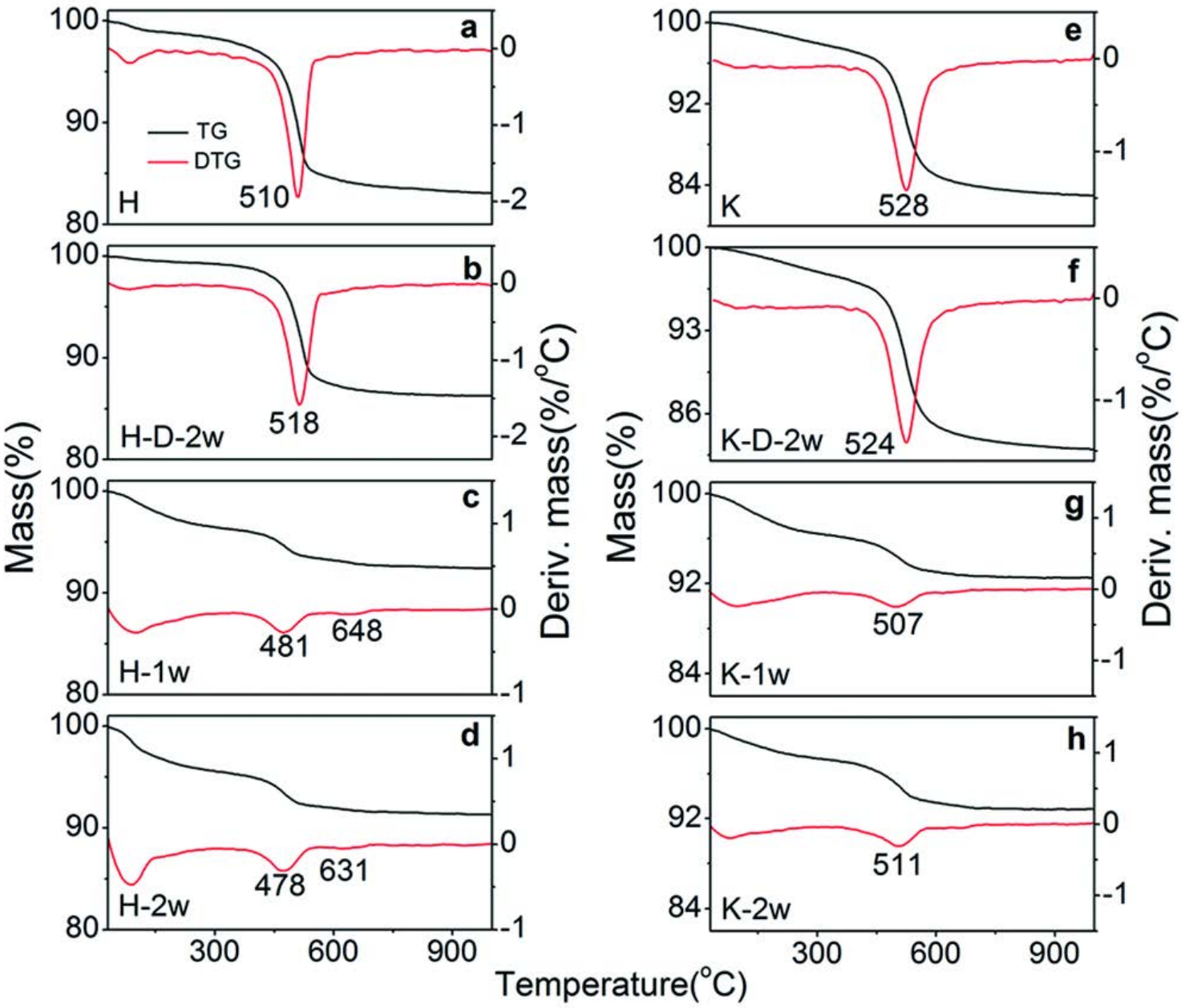

This is a preprint, the final version is subject to change, of the American Mineralogist (MSA)
Cite as Authors (Year) Title. American Mineralogist, in press.
(DOI will not work until issue is live.) DOI: http://dx.doi.org/10.2138/am-2017-5935

Figure 6

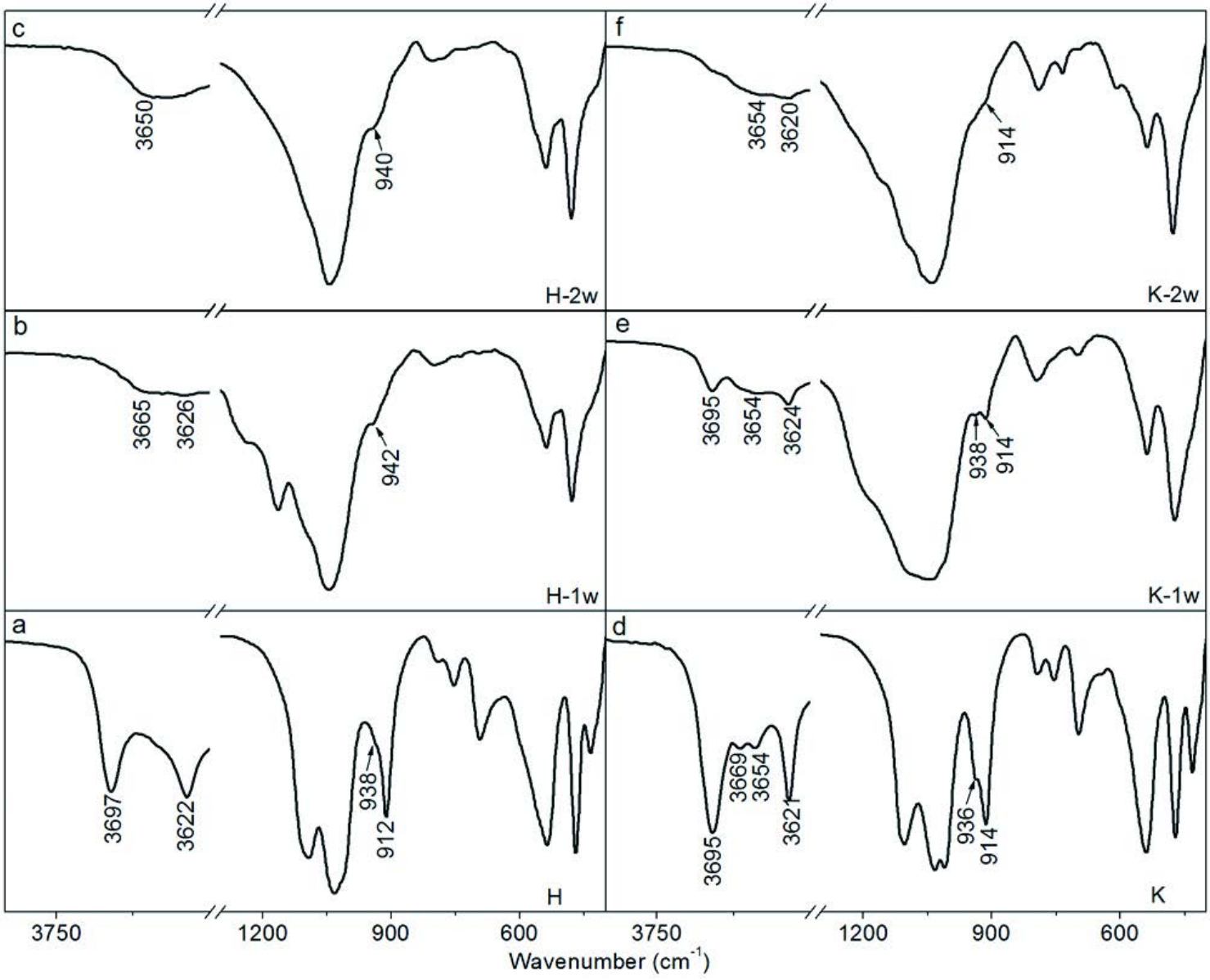

This is a preprint, the final version is subject to change, of the American Mineralogist (MSA)
Cite as Authors (Year) Title. American Mineralogist, in press.
(DOI will not work until issue is live.) DOI: http://dx.doi.org/10.2138/am-2017-5935

Figure 7

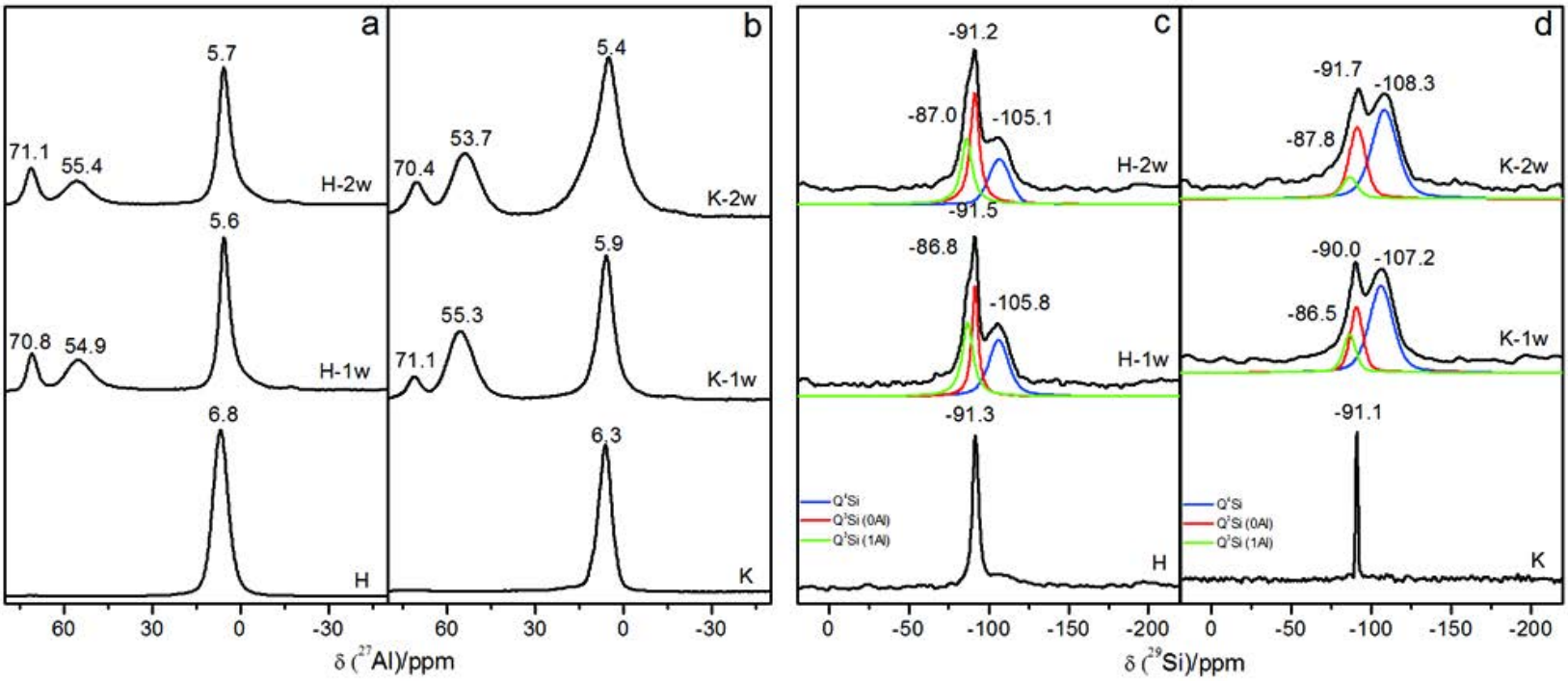

This is a preprint, the final version is subject to change, of the American Mineralogist (MSA)
Cite as Authors (Year) Title. American Mineralogist, in press.
(DOI will not work until issue is live.) DOI: http://dx.doi.org/10.2138/am-2017-5935

Figure 8